

SUPPORTING INFORMATION MATERIAL

for
**Synthesis of Metal-Substituted Tetraalkylphosphonium Polyoxometalate Ionic
Liquids**

Filipe M. Santos, Sandra P. Magina, Helena I. S. Nogueira and Ana M. V. Cavaleiro

Department of Chemistry/CICECO, University of Aveiro, 3810-193 Aveiro, Portugal



Fig. S1. – Picture of $(\text{THTP})_4[(\text{PW}_{11}\text{O}_{39}\text{Mn}^{\text{III}}(\text{H}_2\text{O}))]$ 3 after heated with the flask tilted and then with the flask back again in a vertical position.

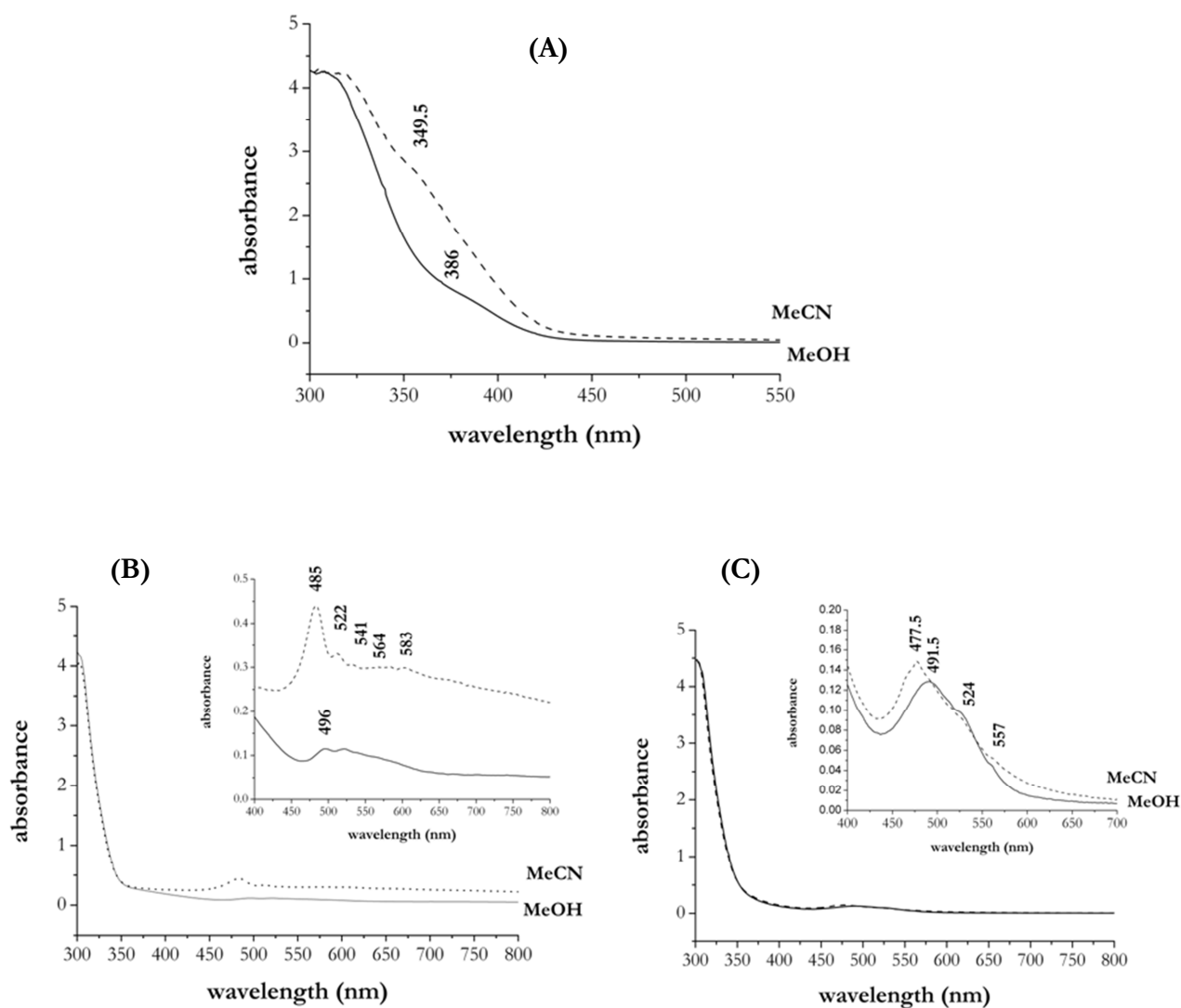


Fig. S2. – UV-vis spectra of (A) $(\text{THTP})_4[\text{PW}_{11}\text{O}_{39}\text{Fe}^{\text{III}}(\text{H}_2\text{O})]$ 1; (B) $(\text{THTP})_5[(\text{PW}_{11}\text{O}_{39}\text{Co}^{\text{II}}(\text{H}_2\text{O}))]$ 2; (C) $(\text{THTP})_4[(\text{PW}_{11}\text{O}_{39}\text{Mn}^{\text{III}}(\text{H}_2\text{O}))]$ 3 in methanol and acetonitrile, respectively ($C = 1.0 \times 10^{-3}\text{M}$).

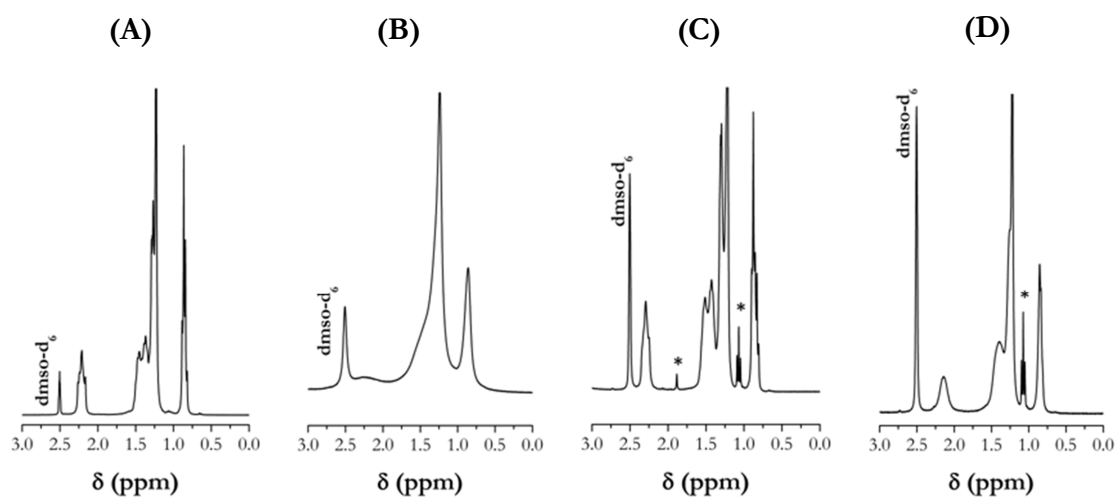


Fig. S3. – ^1H NMR spectra, in dmsO-d_6 , of (A) THTPBr , (B) $(\text{THTP})_4[(\text{PW}_{11}\text{O}_{39}\text{Fe}^{\text{III}}(\text{H}_2\text{O}))]$ 1, (C) $(\text{THTP})_5[(\text{PW}_{11}\text{O}_{39}\text{Co}^{\text{II}}(\text{H}_2\text{O}))]$ 2 and (D) $(\text{THTP})_4[(\text{PW}_{11}\text{O}_{39}\text{Mn}^{\text{III}}(\text{H}_2\text{O}))]$ 3. (*) indicates an impurity found on the tube.

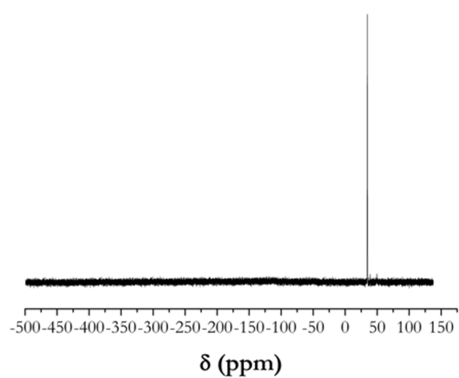


Fig. S4. – ^{31}P NMR spectrum of $(\text{THTP})_5[(\text{PW}_{11}\text{O}_{39}\text{Co}^{\text{II}}(\text{H}_2\text{O}))]$ 2 in dmsO-d_6 .

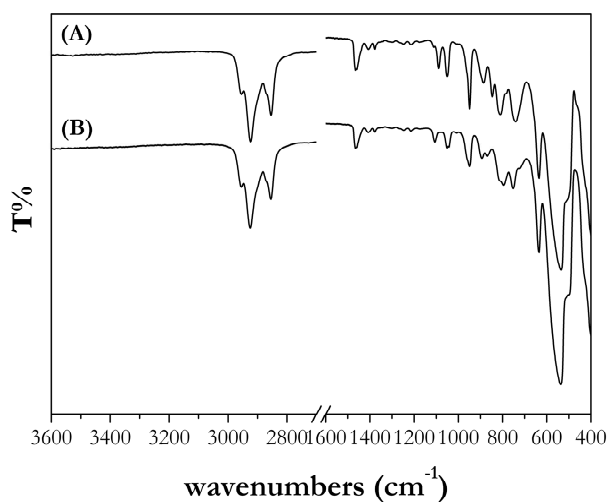


Fig. S5. – FTIR-ATR spectra of (A) $(\text{THTP})_7[\text{PW}_{11}\text{O}_{39}]$ (4) and (B) $(\text{THTP})_{10}[\text{P}_2\text{W}_{20}\text{O}_{70}]$ (5).

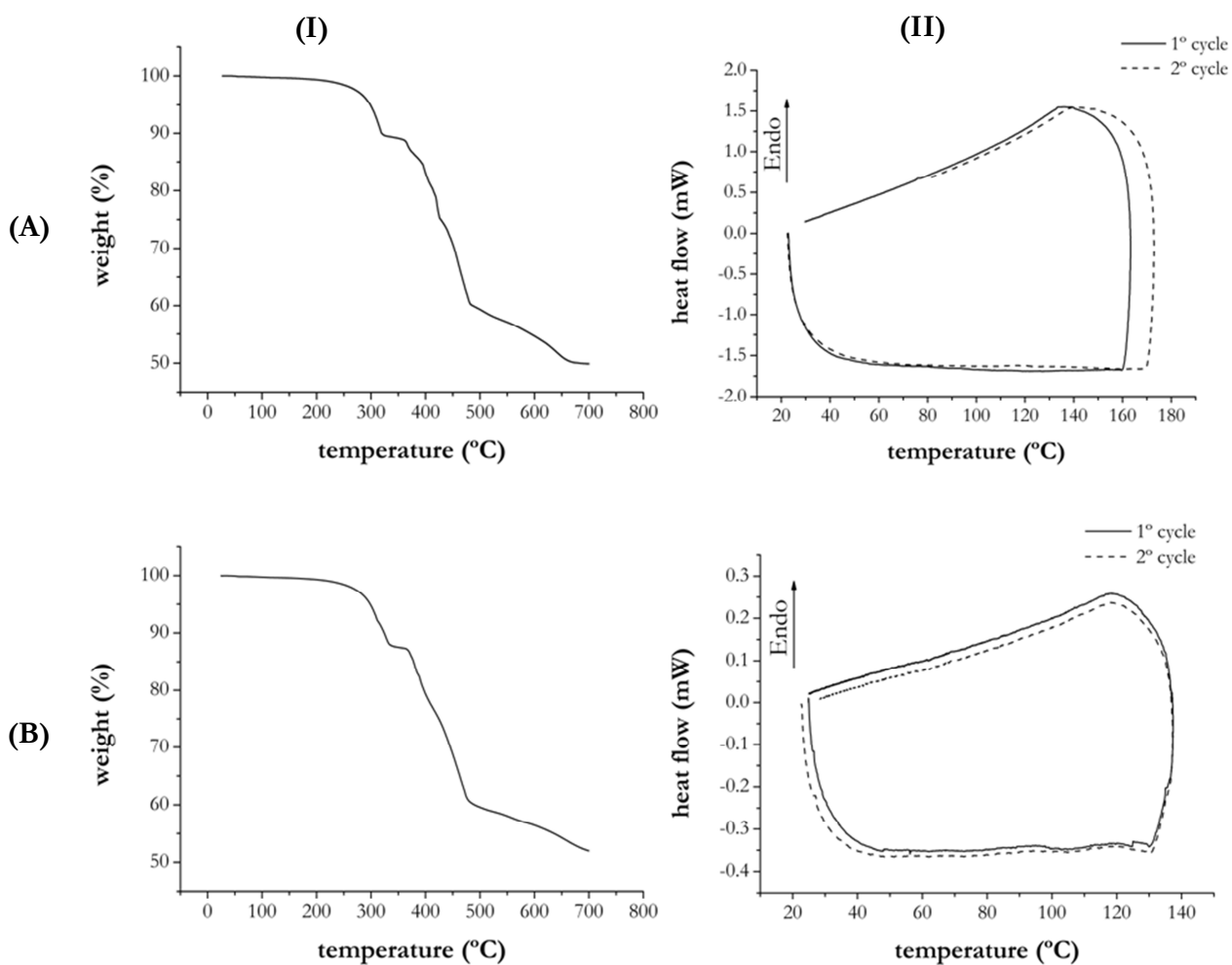


Fig. S6. – Thermal analyses performed on (A) $(\text{THTP})_5[\text{PW}_{11}\text{O}_{39}\text{Co}^{\text{II}}(\text{H}_2\text{O})]$ 2 and (B) $(\text{THTP})_4[\text{PW}_{11}\text{O}_{39}\text{Mn}^{\text{III}}(\text{H}_2\text{O})]$ 3. In I, the thermogravimetric curves are presented and in II, the DSC curves.

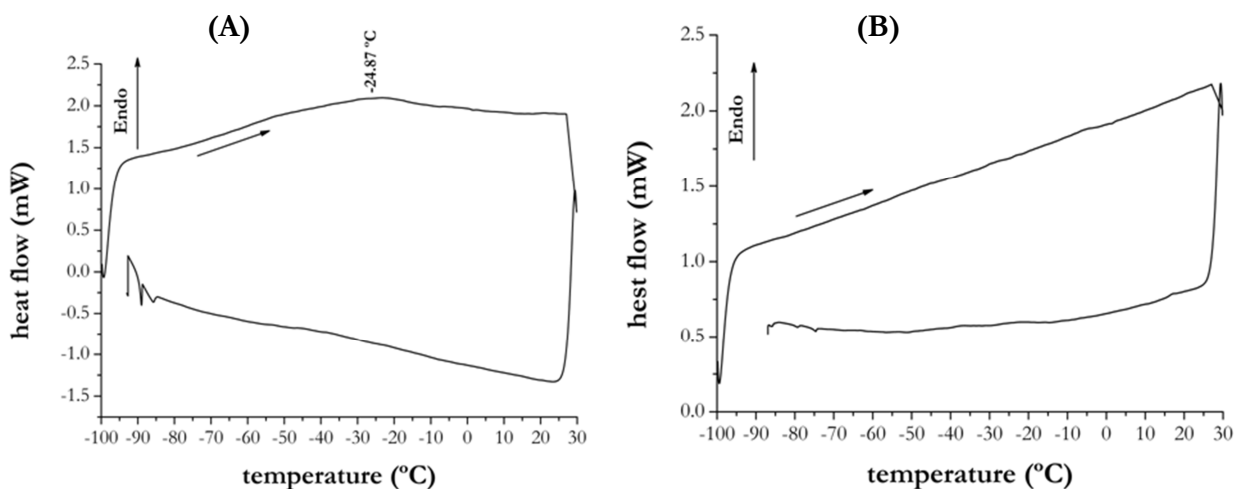


Fig. S7. – DSC plots for (A) $(\text{THTP})_5[\text{PW}_{11}\text{O}_{39}\text{Co}^{\text{II}}(\text{H}_2\text{O})]$ 2; (B) $(\text{THTP})_4[\text{PW}_{11}\text{O}_{39}\text{Mn}^{\text{III}}(\text{H}_2\text{O})]$ 3, between $-100\text{ }^{\circ}\text{C}$ and $+30\text{ }^{\circ}\text{C}$. Heating rate: $-10\text{ }^{\circ}\text{C}\cdot\text{min}^{-1}$.

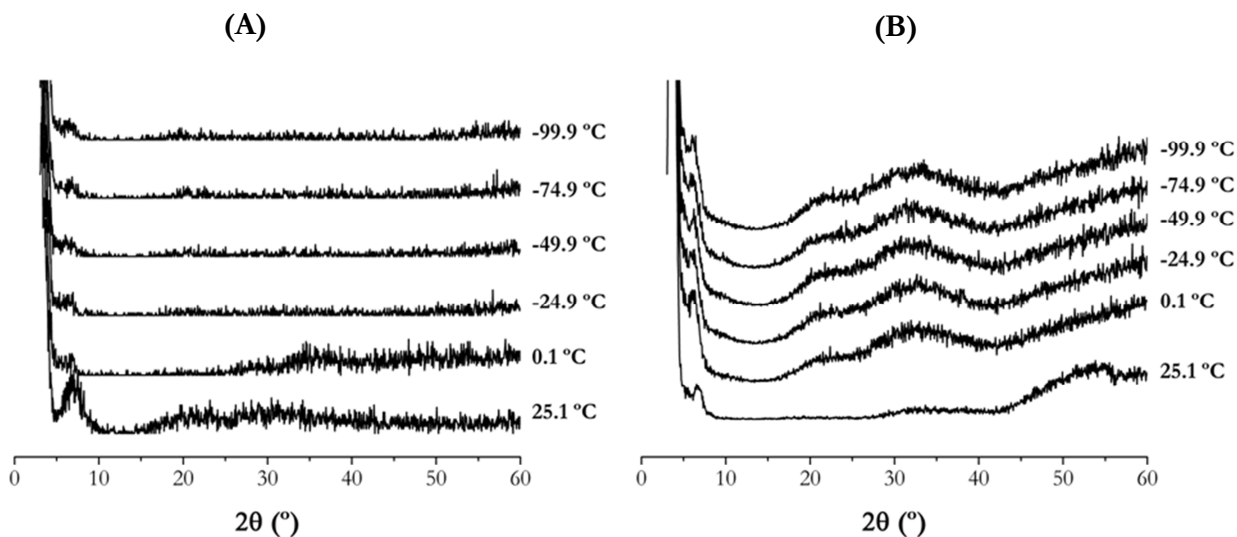


Fig. S8. – X-ray patterns for (A) $(\text{THTP})_4[\text{PW}_{11}\text{O}_{39}\text{Fe}^{\text{III}}(\text{H}_2\text{O})]$ 1; (B) $(\text{THTP})_5[(\text{PW}_{11}\text{O}_{39}\text{Co}^{\text{II}}(\text{H}_2\text{O}))]$ 2, between -100 °C and +25 °C. Heating rate: $-5\text{ }^\circ\text{C}\cdot\text{min}^{-1}$.

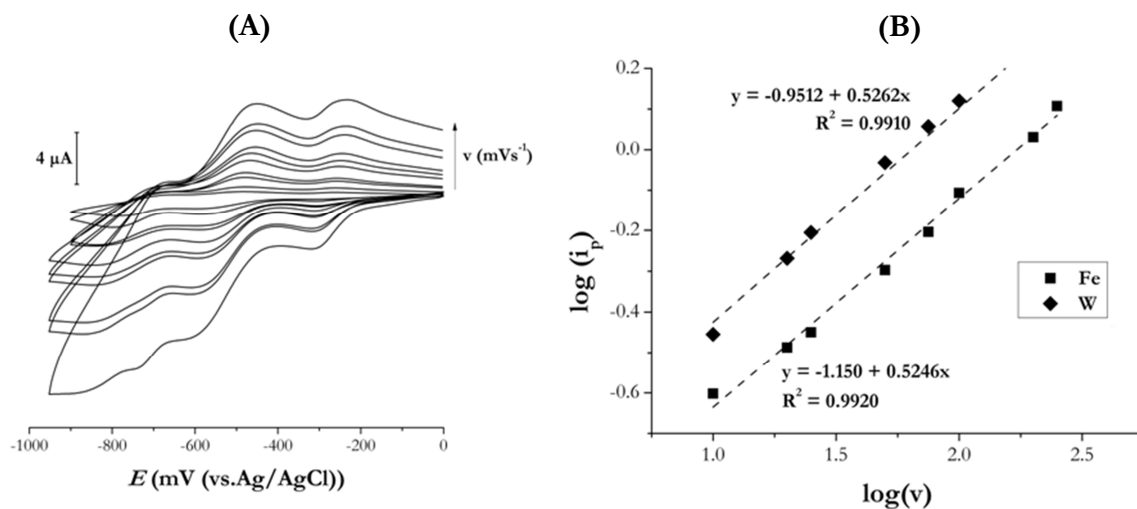


Fig. S9. – Variation of the electrochemical signal of (1) for a pH 2.0 solution. (A) cyclic voltammograms for $v = 5, 10, 20, 25, 50, 75, 100, 200, 250$ and 500 mV s^{-1} ; (B) slopes of $(i_p) = f(\log v)$ for the $\text{Fe}^{\text{III}}/\text{Fe}^{\text{II}}$ and the first $\text{W}^{\text{VI}}/\text{W}^{\text{V}}$ redox pairs for scanning rates between 10 and 100 mV s^{-1} .